ACS Sustainable Chemistry & Engineering

Research Article

Cite This: ACS Sustainable Chem. Eng. XXXX, XXX, XXX−XXX

pubs.acs.org/journal/ascecg

Computational Evidence for Kinetically Controlled Radical Coupling during Lignification

Terry Z. H. Gani,[†] Michael J. Orella,[†] Eric M. Anderson,[†] Michael L. Stone,[†] Fikile R. Brushett,[†] Gregg T. Beckham,*[,‡] and Yuriy Román-Leshkov*[,†]

[†]Department of Chemical Engineering, Massachusetts Institute of Technology, 25 Ames Street, Cambridge, Massachusetts 02139, United States

[‡]National Bioenergy Center, National Renewable Energy Laboratory, 15013 Denver West Parkway, Golden, Colorado 80401, United States

Supporting Information

ABSTRACT: Lignin is an alkyl−aromatic biopolymer that, despite its abundance, is underutilized as a renewable feedstock because of its highly complex structure. An approach to overcome this challenge that has gained prominence in recent years leverages the plasticity and malleability of lignin biosynthesis to tune lignin structure in planta through genetic approaches. An improved understanding of lignin biosynthesis can thus provide fundamental insights critical for the development of effective tailoring and valorization strategies. Although it is widely accepted that lignin monomers and growing chains are oxidized enzymatically into radicals that then undergo kinetically controlled coupling in planta, direct experimental evidence has been scarce because of the difficulty of exactly replicating in planta lignification conditions. Here, we computationally investigate a set of radical reactions representative of lignin biosynthesis. We show that, contrary to the notion that radical coupling reactions are usually barrierless and dynamically controlled, the computed activation energies can be qualitatively consistent with key structural observations made empirically for native lignin in a variety of biomass types. We also rationalize the origins of regioselectivity in coupling reactions through structural and activation strain analyses. Our findings lay the groundwork for first-principles lignin structural models and more detailed multiscale simulations of the lignification process.

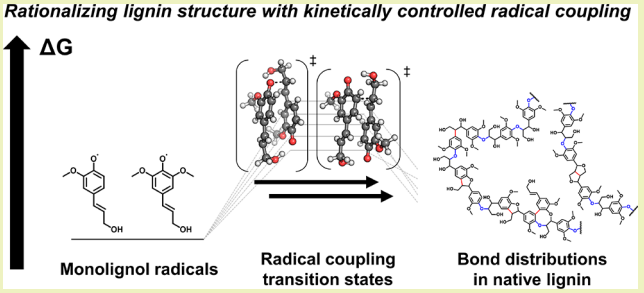

KEYWORDS: *Lignin biosynthesis, Lignin structure, Density functional theory, Polymerization, Radical coupling*

INTRODUCTION

Lignin is an abundant alkyl−aromatic biopolymer constituting up to 30% by weight of biomass[1] that strengthens cell walls, facilitates water transport, and inhibits microbial attack.[2] It is composed mainly of phenylpropanoid building blocks (i.e., monolignols) that give rise to eight known C−O or C−C linkages of widely varying strengths and characteristics.[2−4] Lignin offers tremendous potential value as a renewable resource[5] for bulk chemical,[6−8] specialty chemical,[9] and functional polymer[10] production, particularly if it can be efficiently depolymerized into monomeric units rather than lower value oligomeric fractions or pyrolysis oil.[11] This is a formidable challenge primarily because of the high degree of structural complexity[2−4] that limits achievable monomer yields of selective depolymerization strategies,[12,13] notably those targeting the most abundant and labile β−O−4 (alkyl aryl ether) linkages.[14] On the basis of statistical arguments alone, monomer yields should increase with the proportion of β−O−4 linkages,[15,16] which should in turn be related to the method of lignin extraction[5] and the relative proportions of monomeric units with different propensities to form β−O−4 bonds.[4] However, recent experiments have revealed surprising exceptions to this rule, notably invariance of monomer yields to monolignol composition across native poplar variants[17] and oxidative depolymerization yields that do not track with β−O−4 content across lignins extracted from various biomass types,[18] that motivate detailed structural investigations for rationalizing these discrepancies and informing the development of more efficient depolymerization processes.

Plants produce lignin by polymerizing a small slate of monolignols that are biosynthesized in the cytoplasm[2−4] and transported to the cell wall through mechanisms that are not yet well understood.[19] In the cell wall, laccase and peroxidase enzymes facilitate the oxidation of the monolignols and the growing oligomeric chains into phenoxyl radicals. It is widely accepted that chain growth occurs by kinetically controlled radical coupling, followed by aromaticity-restoring tautomerization and/or hydration, as demonstrated by the lack of optical

Received: May 6, 2019
Revised: June 24, 2019
Published: July 5, 2019

DOI: 10.1021/acssuschemeng.9b02506
ACS Sustainable Chem. Eng. XXXX, XXX, XXX−XXX

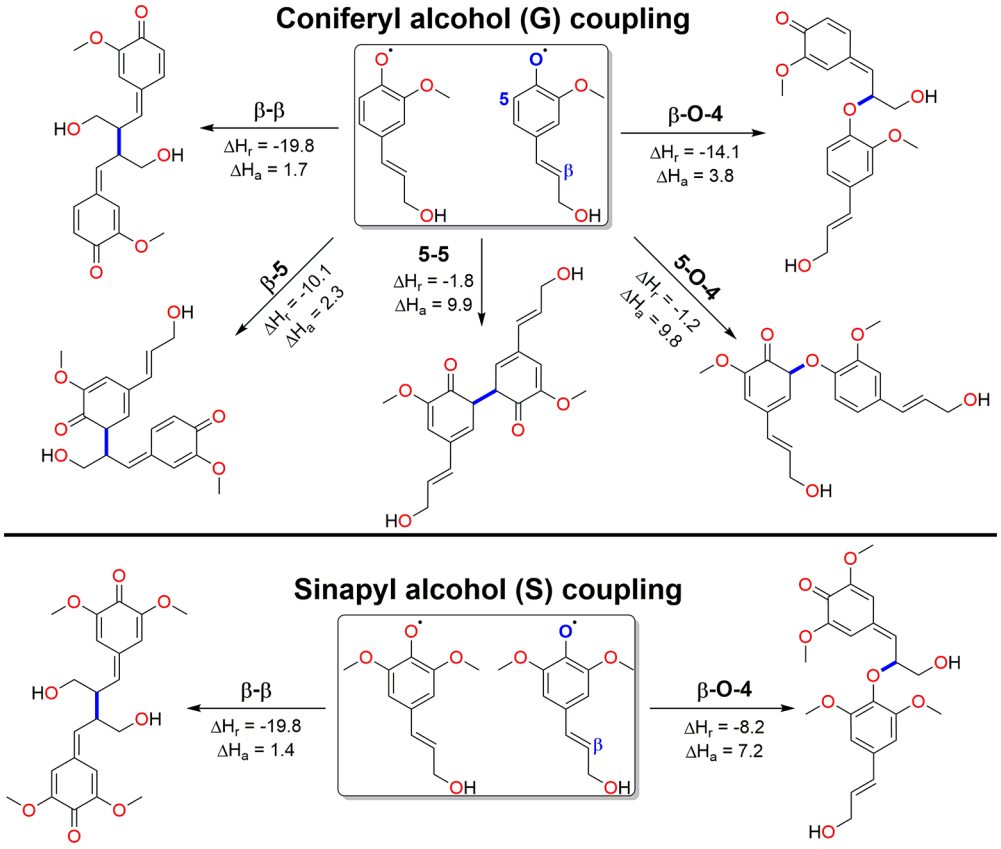

Figure 1. Monolignols and monolignol coupling reactions studied in this work. Each reaction is labeled with its reaction enthalpy (ΔH_r, kcal/mol) and activation enthalpy (ΔH_a, kcal/mol). Reactive positions of monomers and bonds formed in each coupling product are labeled in blue. Results obtained with other density functionals and coupled-cluster theory are presented in SI Table S1.

activity in lignin[20] and the ease of incorporating nonstandard monolignols into growing chains.[21] While empirical structural models have been developed[22−27] and successfully used to predict product distributions from lignin pyrolysis,[28] their usefulness is limited by the accuracy of the underlying experimentally measured analytical properties that they are designed to reproduce. Inconsistencies among experimental data sources have necessitated empirical parameter tuning in some of these models, which limits predictive capabilities.[27] The development of predictive, first-principles structural models[29] has so far been hindered by the complexity of lignin biosynthesis, which involves a complex, spatiotemporally controlled interplay of metabolic pathways, monomer transport, and enzymatic and nonenzymatic polymerization reaction steps.[30] Due to challenges in studying lignification in planta at the molecular scale, conclusive evidence for kinetically controlled radical coupling has been scarce in the open literature. In vitro polymerization experiments[31−37] have shed light on lignin polymerization mechanisms but are inherently limited by the historical difficulty of quantifying complex product mixtures and the inability to fully replicate in planta lignification conditions.

In this regard, first-principles calculations can provide valuable, complementary insight. For instance, extensive study of the thermochemical properties of lignin linkages[38−46] has helped to rationalize the relative lability of the β−O−4 linkage[23] and the effect of partial oxidation of the β−O−4 linkage on delignification efficiency.[47] However, with few exceptions,[48] computational studies of lignin polymerization have so far been limited to the thermodynamics[49,50] of monolignol coupling reactions or the kinetics[51,52] of β−O−4 coupling, neither of which provide a complete picture of the chemical reactions occurring during lignification. We note that during radical coupling, spin delocalization throughout the conjugated carbon framework of each radical gives rise to a multitude of reactive sites[50] and possible coupling products. As such, the relative proportions and sequences of observed linkages would then be governed by a combination of the relative propensities of radical coupling at each reactive site and the relative concentrations of reactive intermediates.[4] Therefore, adequate first-principles models of lignin structure can be developed by quantifying radical coupling and product formation rates.[29] In this work, we take a step toward such a model by computing the activation barriers of a representative set of radical formation and coupling reactions and showing that they generally agree with qualitative experimental observations of lignin structure. Our work thus provides a foundation for more extensive multiscale simulations of the lignification process.

COMPUTATIONAL METHODS

The computational methods are described fully in the Supporting Information (SI). Briefly, all density functional theory (DFT) calculations were performed using ORCA 4.0.1.[53] Geometries were optimized at the B3LYP[54−56]-D3[57]/def2-SV(P)[58] level of theory, and single-point energies were calculated at the M06-2X[59]/def2-TZVP[58] level of theory, which has been shown to perform well for the thermochemistry of lignin models.[40] Although DFT-calculated reaction energetics can be dependent on the functional used, our qualitative conclusions remain consistent across several functionals

DOI: 10.1021/acssuschemeng.9b02506
ACS Sustainable Chem. Eng. XXXX, XXX, XXX−XXX

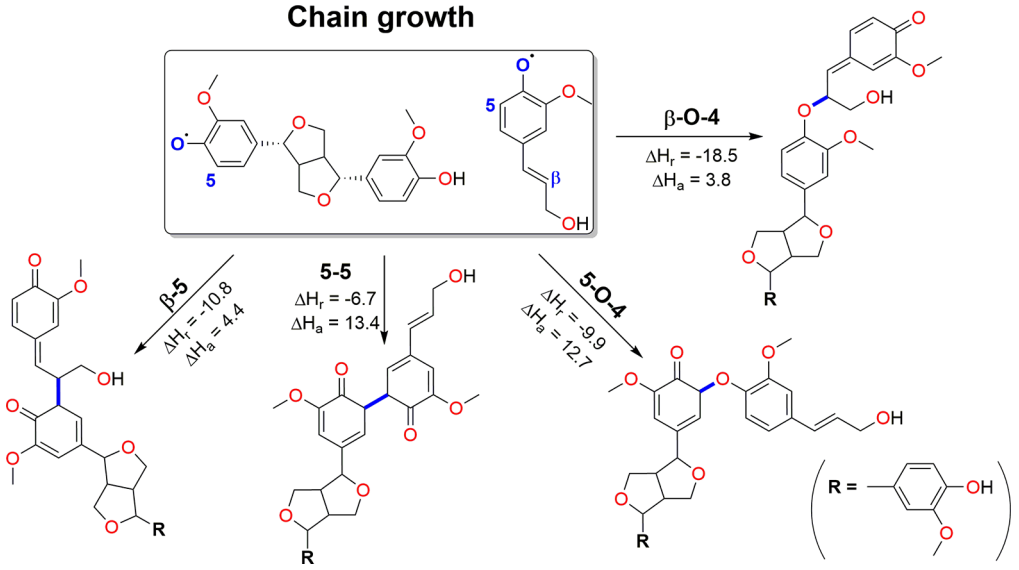

Figure 2. Representative chain growth reactions. Each reaction is labeled with its reaction enthalpy (ΔH_r, kcal/mol) and activation enthalpy (ΔH_a, kcal/mol). Reactive positions of coupling units and bonds formed in each coupling product are labeled in blue. Results obtained with other density functionals and coupled-cluster theory are presented in SI Table S2.

and coupled-cluster theory as they are based on relative reaction rates that are usually more invariant to functional choice (SI Tables S1−S4 and vide infra). Solvation contributions were treated implicitly with the CPCM model,[60] and the choice of water (ε = 80.4) as the solvent was motivated by the aqueous environments of in planta and in vitro polymerizations. Lignin polymerization is unique among biological reactions in that enzymes are thought not to be involved in the radical coupling and transfer steps that govern lignin structure. As one of the goals of this work was to investigate if such a model is consistent with experimental observations of lignin structure, we accordingly modeled these steps in the absence of protein interactions. Considering further the lack of significant charge separation along the reaction coordinates, we believe an implicit solvent approach to be adequate for understanding the intrinsic selectivities of these steps as they occur in the developing plant cell wall. As rigorous conformational analyses[61] of large and flexible oligomers are computationally intractable, we instead identified a single lowest energy conformer for each reaction by DFT optimizing structures obtained from force field-based searches, as in prior studies.[40,50] Future work will focus on explicit consideration of dynamic, solvation, and confinement effects for predicting the structure of growing lignin chains. All calculations were spin unrestricted, and transition states were located by scanning the singlet and broken-symmetry spin surfaces along the radical coupling reaction coordinates, followed by eigenvector following optimizations from the energy maxima. Although necessary for accurate absolute rate predictions, entropic contributions to activation energies were not included owing to the difficulty of accurate estimation in solution.[62] We nevertheless note that all coupling reactions will have a positive entropy of activation that further contributes to their barriers in solution.

RESULTS AND DISCUSSION

Monolignol Radical Coupling. The complex interlinked networks of sinapyl alcohol (S) and coniferyl alcohol (G) monomeric units found in the lignin structure of most biomass types begin from the simple dimerization of two monolignols. Some biomass types (e.g., softwoods and grasses, but not hardwoods) also contain a third monolignol, *p*-coumaryl alcohol (H), but only in very small amounts.[4] Accordingly, peroxidase-catalyzed bulk dehydrogenation polymerization (DHP) of S and G monomers, in which dimerization is the dominant process, has been extensively investigated in vitro. As illustrated in Figure 1, the G monomer has 3 reactive sites (β, 5, and O−4) that give rise to 5 possible self-coupling products: β−β, β−O−4, β−5, 5−5, and 5−O−4, excluding O−O that yields an extremely unstable peroxide. The S monomer has 2 reactive sites (β and O−4; the 5 position is occupied by a methoxy group that blocks subsequent rearomatization) that give rise to 2 possible self-coupling products: β−β and β−O−4. These coupling products do not include several linkages found in native lignin (e.g., α−O−4, which requires a chain propagation step, and β−1, which requires a preformed β−O−4 linkage) because they are not derived from simple coupling of monolignol radicals.[4] As a first test of the relevance of kinetically controlled radical coupling to lignification, we begin by comparing experimentally observed product distributions of these in vitro dimerization experiments to computed relative radical coupling activation energies. We focus on the initial radical coupling step as under lignification conditions the direct radical coupling products, known as quinone methides, are metastable intermediates that subsequently undergo highly exothermic and irreversible[50] hydration and tautomerization steps to restore aromaticity. These steps are also responsible for the complexity and diversity of bond types (e.g., resinols from β−β coupling, phenylcoumarans from β−5 coupling, and spirodienones from β−1 coupling) in native lignins.[4] Accordingly, the coupling products illustrated in Figures 1, 2, and 4 depict the quinone methide intermediates instead of these equilibrium linkage structures.

We observe differences in activation energies among coupling products that are in general agreement with product distributions from in vitro dimerizations.[32,35] Notably, G−G couplings involving the β position (β−β, β−5, and β−O−4) have comparable barriers (ca. 2−4 kcal/mol) that are much smaller than the corresponding barriers for 5−5 and 5−O−4 couplings (ca. 10 kcal/mol) (Figure 1, top). Indeed, horseradish peroxidase (HRP)-catalyzed DHP of G monomers in aqueous solution yields a mixture of β−β, β−5, and β−O−4 dimers in comparable amounts.[32,35] The relative barriers of β−β, β−5, and β−O−4 couplings are somewhat sensitive to functional choice, but the 5−5 and 5−O−4 couplings are

DOI: 10.1021/acssuschemeng.9b02506
ACS Sustainable Chem. Eng. XXXX, XXX, XXX−XXX

strongly disfavored across multiple levels of theory (SI Table S1). Further, the ca. 2 kcal/mol difference in activation energies between $\beta-\beta$, $\beta-5$, and $\beta-O-4$ couplings is within standard computational error, and dynamic effects that are outside the scope of this work may further contribute to the selectivities. Importantly, radical coupling thermodynamics alone do not accurately describe selectivity, greatly overpredicting the favorability of $\beta-\beta$ linkages, thus necessitating explicit consideration of individual activation energies over simpler empirical relationships that relate thermodynamics to kinetics.[63,64] Interestingly, addition of methoxy groups to the G units disfavors $\beta-O-4$ coupling but not $\beta-\beta$ coupling, exhibiting a larger difference in barrier heights for the S−S coupling reactions (ca. 1.4 kcal/mol for $\beta-\beta$ coupling vs 7.2 kcal/mol for $\beta-O-4$ coupling) (Figure 1, bottom). This is again consistent with experimental observations of primarily the $\beta-\beta$ dimer in bulk DHP of S monomers.[31,35] While we recognize that the computed energetic differences are small, results obtained with other density functionals and coupled-cluster theory presented in SI Table S1 are also in full agreement with our observations.

The notion of kinetically controlled radical coupling appears to contradict the expectation that, excluding the positive free energy contribution from the negative entropy of reaction, radical coupling reactions should be intrinsically barrierless[65] because the interaction of two singly occupied molecular orbitals (SOMOs) should produce a doubly occupied MO that is more stable than either SOMO. Although small radical coupling barriers can sometimes result from disruption of intermolecular forces in the reacting complex (RC),[65] this is not the case here as the relative monomer orientations are preserved along the bond-forming reaction coordinates (SI Figure S1). We thus applied the distortion-interaction activation strain model (ASM)[66] to better understand from first-principles this unexpected observation. ASM decomposes the relative electronic energy, ΔE, at any point along a reaction coordinate into a strain component, ΔE_{str}, corresponding to the energy required to distort the reacting monomeric fragments from their RC geometry to their current geometry and an interaction component, ΔE_{int}, corresponding to the stabilization when the fragments interact at this geometry, i.e.,

$$\Delta E = \Delta E_{str} + \Delta E_{int} \quad (1)$$

As ΔE_{str} is always positive and ΔE_{int} is always negative, a transition state (TS) will result only if their rates of change balance each other somewhere along the reaction coordinate,[66] and this is indeed the case for all coupling positions (Table 1). Although reactivity differences can sometimes be rationalized solely by differences in the contributions of either component,[67] we find that this is not the case here. For instance, the $\beta-\beta$ reaction is most favorable overall despite its relatively large strain energy, and $\beta-O-4$ is much more favorable than 5−O−4 despite both reactions having comparable interaction energies. Rather, the observed regioselectivity of monolignol radical coupling appears to be controlled by a delicate balance between strain and interaction. Reactions at the β and 5 positions experience greater strain than reactions at the O−4 position because pyramidalization of the C atoms disrupts π orbital conjugation and orbital overlap with adjacent atoms. At the β position, this increase in ΔE_{str} is compensated by a more favorable interaction energy arising from an increase in C 2p character of the SOMO that enhances spatial orbital overlap during bond formation (SI Figure S2).

Table 1. Strain (ΔE_{str}) and Interaction (ΔE_{int}) Contributions (in kcal/mol) to the TS and Product Energies of Radical Coupling Reactions[a]

		transition state		product	
monomers	linkage	ΔE_{int}	ΔE_{str}	ΔE_{int}	ΔE_{str}
G−G	$\beta-\beta$	−5.9	8.1	−82.7	60.4
G−G	$\beta-5$	−3.3	5.9	−65.7	53.6
G−G	5−5	−0.6	10.5	−55.3	51.7
G−G	$\beta-O-4$	−0.6	6.2	−53.3	39.0
G−G	5−O−4	−0.3	10.0	−43.4	40.6
S−S	$\beta-\beta$	−9.3	12.4	−85.9	63.9
S−S	$\beta-O-4$	−1.3	9.2	−54.3	44.9

[a]Plots of ΔE, ΔE_{int}, and ΔE_{str} along the bond-forming reaction coordinates are provided in SI Figure S3.

The unusually low strain contribution to the $\beta-5$ reaction is attributable to a second hydrogen bond that enforces geometric similarity between the RC, TS, and product (SI Figure S1).

Chain Growth. Known discrepancies between the structures of synthetic DHP products and native lignin motivate consideration of chain growth reactions (i.e., cross-coupling between monolignol and oligolignol radicals) and monomer addition rates (ref 68 and vide infra) in addition to monolignol coupling reactions. Notably, there are too few $\beta-O-4$ linkages in most DHPs because monolignol dimerization and its dominant $\beta-\beta/\beta-5$ coupling modes are overrepresented,[4] as evidenced by the strong dependence of cross-coupling selectivity on the rate of monomer addition.[36] Furthermore, the strong preference for addition to the O−4 position of the growing chain over the 5 position[36,69] suggests an intrinsic difference in regioselectivities of monolignol coupling and chain growth beyond the inability of the oligolignol (growing chain) radical to couple at its β position and explains why $\beta-O-4$ is the dominant linkage even in softwood (i.e., high G) lignins.[4] Thus, to evaluate the ability of kinetically controlled radical coupling to qualitatively predict these reactivity differences, we investigated the coupling of a G radical to a representative G−G $\beta-\beta$ resinol dimer (Figure 2). In accordance with our expectations, we observe a slight preference for $\beta-O-4$ coupling over $\beta-5$ coupling (ca. 3.8 vs 4.4 kcal/mol), with 5−O−4 and 5−5 coupling remaining highly unfavorable. Although well within standard computational error, this preference is nevertheless consistent with the magnitude of the experimentally observed $\beta-O-4$ selectivity (e.g., a 1 kcal/mol difference in barriers corresponds to an 85:15 ratio of relative rates at 25 °C) while also persisting across multiple levels of theory, albeit with variations in magnitude (SI Table S2).

Radical Transfer. The high propensity for chain growth in native lignin appears at first glance to be inconsistent with our calculations that reveal small differences between chain growth and monomer coupling barrier heights but is in fact fully consistent with the longstanding hypothesis that the relative rates of monomer coupling and chain growth are governed by differences between the concentrations of monolignol and oligolignol radicals.[4,70] Indeed, chain growth and concomitant formation of labile $\beta-O-4$ linkages can be favored in DHP experiments by decreasing the rate of monolignol addition,[33,36] decreasing the peroxidase concentration,[71] introducing alternative peroxidases with enhanced affinities for growing chains,[70,72] or increasing the solubility of growing chains,[37]

DOI: 10.1021/acssuschemeng.9b02506
ACS Sustainable Chem. Eng. XXXX, XXX, XXX−XXX

all of which promote the formation of oligolignol radicals over monolignol radicals. These observations highlight the importance of determining rates of radical formation in addition to the rates of radical coupling in first-principles kinetic models of lignification.

To this end, it was recently shown that, notwithstanding enzyme-binding effects, experimentally observed monolignol and dilignol reactivities toward HRP were correlated to the p orbital density of the phenolic oxygen.[48] Encouraged by this result, we computed activation energies for radical transfer from a methyl *p*-coumarate radical to representative G and S monolignols and dilignols in order to further shed light on their relative propensities for radical formation (Figure 3).

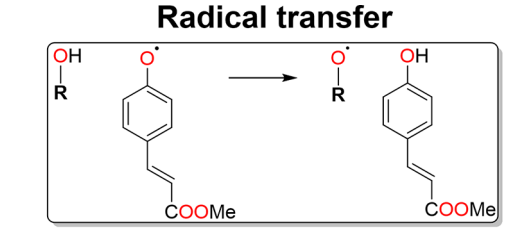

–R	BDE	ΔH_a
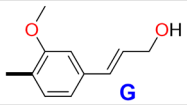 G	83.7	0.5
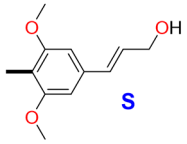 S	79.8	-0.3
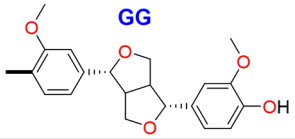 GG	85.4	3.9
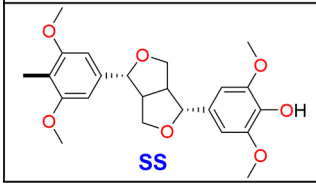 SS	81.8	4.4

Figure 3. Representative radical transfer reactions. Boldface lines depict how the O–H bonds broken during radical transfer are linked to the remainder of the lignin unit (i.e., the –R group in the schematic above). Each substrate is tabulated with its O–H bond dissociation energy (BDE, kcal/mol) and radical transfer activation enthalpy (ΔH_a, kcal/mol). O–H BDEs do not correlate well with radical transfer kinetics, suggesting that monolignol reactivity is primarily kinetic in origin. Results obtained with other density functionals and coupled-cluster theory are presented in SI Table S3.

Besides quantifying intrinsic dehydrogenation reactivities, these reactions also reasonably depict lignification in herbaceous feedstocks in which both growing chains as well as monolignols are oxidized primarily by radical transfer from *p*-coumarates rather than directly by enzymes.[73] Our calculations confirm that radical transfers to monolignols are highly facile (Figure 3 and SI Table S3). Analysis of TS geometries and electronic structures revealed that noncovalent interactions including π stacking favor asynchronous hydrogen atom transfer (HAT) reactions over stepwise proton-coupled electron transfers that would be more characteristic of phenoxyl radicals[74] (SI Figure S4). More importantly, we also found that radical transfers to growing chains are less efficient than to monolignols, thus necessitating a slow monomer addition rate to achieve reasonable chain lengths in the absence of external factors that specifically promote the oxidation of growing chains. To this effect, oligolignol-specific peroxidases have been identified in hardwoods[72] and softwoods[70] that may help ease the requirement for very slow monomer addition, which would ostensibly also lead to very slow lignification rates. In herbaceous lignins, extensive ferulate cross-linking[75] may also serve to reduce the number of difficult growing chain oxidations required for lignification. We further hypothesize that the recently noted inability of 5–O–4 and 5–5 linkages to undergo chain branching reactions in softwoods[76] can similarly be explained by an intrinsic lack of reactivity toward HAT reactions, and work along these lines is ongoing.

Growing Chain Coupling. The small but significant fractions of 5–O–4 and 5–5 linkages (ca. 1%[76] and 3–4%,[77,78] respectively) present in native softwood lignin pose a final test for kinetically controlled radical coupling, as their orders of magnitude are inconsistent with the differences in coupling activation energies calculated so far (e.g., $\Delta\Delta H_a$ of 6 kcal/mol corresponds to a <0.1% ratio of relative rates at 25 °C). As DHP of model dilignols in the absence of monolignols does indeed yield such linkages,[36] it has been hypothesized that they result from the coupling of two growing chains, which can each only react at the 5 or O positions.[2,4,76] These couplings would be vanishingly unlikely in DHP experiments where monolignols can freely diffuse in solution together with growing chains but may be facilitated by spatial confinement or mass-transfer regulation effects under in planta lignification conditions. However, the feasibility of this pathway would require much lower intrinsic barriers for the coupling of two growing chains that would be predicted from monolignol coupling or chain growth. Indeed, we observe low barrier heights (ca. 2–3 kcal/mol) for the 5–5 and 5–O–4 coupling of two pinoresinol units that are comparable to barrier heights for monolignol coupling at the β position, suggesting that growing chains can indeed easily couple if they are both oxidized and suitably oriented (Figure 4 and SI Table S4).

4. CONCLUSIONS

We computed activation energies for a representative set of radical coupling and transfer reactions and, contrary to expectations that radical couplings should be barrierless and dynamically controlled, demonstrated qualitative agreement with key structural observations of native lignin and synthetic dehydrogenation polymers. Overall, our findings provide computational evidence for the role of kinetically controlled radical coupling, in particular the differences between monolignol coupling, chain growth, and oligolignol coupling rates, in the lignification process, thereby complementing decades of experiments on in vitro lignification. Our findings also provide a blueprint toward first-principles lignin structural models: under kinetic control, relative reaction rates can be obtained from our relative activation energies using the Arrhenius equation and, together with monomer addition and radical formation rates, can then be incorporated into kinetic Monte Carlo models of the polymerization process.[29,79] Ongoing work in our groups is focused on investigating spatial and confinement effects not treated in this work through more

DOI: 10.1021/acssuschemeng.9b02506
ACS Sustainable Chem. Eng. XXXX, XXX, XXX–XXX

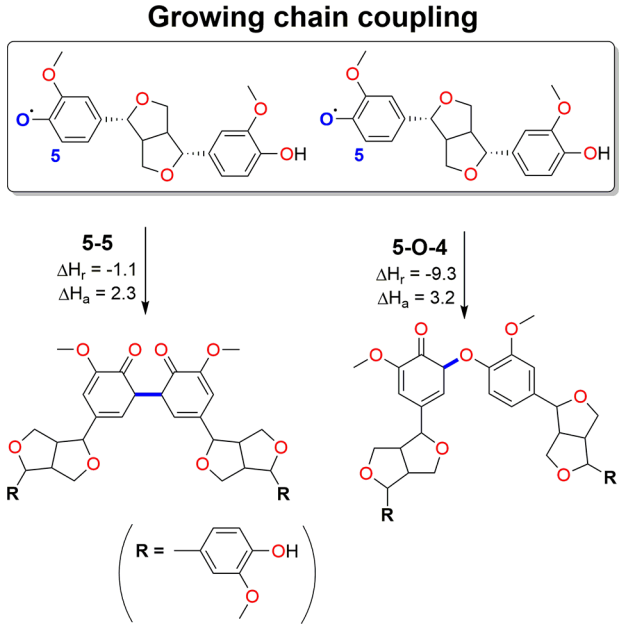

Figure 4. Representative chain-coupling reactions. Each reaction is labeled with its reaction enthalpy (ΔH_r, kcal/mol) and activation enthalpy (ΔH_a, kcal/mol). Reactive positions of coupling units and bonds formed in each coupling product are labeled in blue. Results obtained with other density functionals and coupled-cluster theory are presented in SI Table S4.

sophisticated ab initio dynamic simulations of the lignification process and unraveling the effects of monolignol composition and biosynthetic parameters on lignin structure and depolymerization yields.

■ ASSOCIATED CONTENT

Supporting Information

The Supporting Information is available free of charge on the ACS Publications website at DOI: 10.1021/acssuschemeng.9b02506.

Full computational details; energies and Cartesian coordinates of optimized structures; results with other density functionals and coupled cluster theory; illustrations of RC, TS, and PC geometries; detailed activation strain analyses; MO analyses of radical coupling and transfer TSs (PDF)
(XLSX)
(TXT)

■ AUTHOR INFORMATION

Corresponding Authors

*E-mail: gregg.beckham@nrel.gov.
*E-mail: yroman@mit.edu.

ORCID

Terry Z. H. Gani: 0000-0003-0357-6390
Michael J. Orella: 0000-0003-1207-4704
Fikile R. Brushett: 0000-0002-7361-6637
Gregg T. Beckham: 0000-0002-3480-212X
Yuriy Román-Leshkov: 0000-0002-0025-4233

Notes

The authors declare no competing financial interest.

■ ACKNOWLEDGMENTS

This work was funded by The Center for Bioenergy Innovation, a U.S. Department of Energy Research Center supported by the Office of Biological and Environmental Research in the DOE Office of Science. This work was carried out using computational resources from the Extreme Science and Engineering Discovery Environment (XSEDE), which is supported by National Science Foundation grant no. ACI-1053575, under allocations MCB-090159 and CTS-180027. M.J.O. was supported by the National Science Foundation Graduate Research Fellowship Program (award no. 1122374).

■ REFERENCES

(1) Huber, G. W.; Iborra, S.; Corma, A. Synthesis of Transportation Fuels from Biomass: Chemistry, Catalysts, and Engineering. *Chem. Rev.* **2006**, *106*, 4044−4098.
(2) Vanholme, R.; Demedts, B.; Morreel, K.; Ralph, J.; Boerjan, W. Lignin Biosynthesis and Structure. *Plant Physiol.* **2010**, *153*, 895−905.
(3) Boerjan, W.; Ralph, J.; Baucher, M. Lignin Biosynthesis. *Annu. Rev. Plant Biol.* **2003**, *54*, 519−546.
(4) Ralph, J.; Lundquist, K.; Brunow, G.; Lu, F.; Kim, H.; Schatz, P. F.; Marita, J. M.; Hatfield, R. D.; Ralph, S. A.; Christensen, J. H. Lignins: Natural Polymers from Oxidative Coupling of 4-Hydroxyphenyl-Propanoids. *Phytochem. Rev.* **2004**, *3*, 29−60.
(5) Schutyser, W.; Renders, T.; Van den Bosch, S.; Koelewijn, S.-F.; Beckham, G. T.; Sels, B. F. Chemicals from Lignin: An Interplay of Lignocellulose Fractionation, Depolymerisation, and Upgrading. *Chem. Soc. Rev.* **2018**, *47*, 852−908.
(6) Anderson, E.; Crisci, A.; Murugappan, K.; Román-Leshkov, Y. Bifunctional Molybdenum Polyoxometalates for the Combined Hydrodeoxygenation and Alkylation of Lignin-Derived Model Phenolics. *ChemSusChem* **2017**, *10*, 2226−2234.
(7) Verboekend, D.; Liao, Y.; Schutyser, W.; Sels, B. F. Alkylphenols to Phenol and Olefins by Zeolite Catalysis: A Pathway to Valorize Raw and Fossilized Lignocellulose. *Green Chem.* **2016**, *18*, 297−306.
(8) Cao, Z.; Dierks, M.; Clough, M. T.; Daltro de Castro, I. B.; Rinaldi, R. A Convergent Approach for a Deep Converting Lignin-First Biorefinery Rendering High-Energy-Density Drop-in Fuels. *Joule* **2018**, *2*, 1118−1133.
(9) Sun, Z.; Fridrich, B.; de Santi, A.; Elangovan, S.; Barta, K. Bright Side of Lignin Depolymerization: Toward New Platform Chemicals. *Chem. Rev.* **2018**, *118*, 614−678.
(10) Wang, S.; Shuai, L.; Saha, B.; Vlachos, D. G.; Epps, T. H., III From Tree to Tape: Direct Synthesis of Pressure Sensitive Adhesives from Depolymerized Raw Lignocellulosic Biomass. *ACS Cent. Sci.* **2018**, *4*, 701−708.
(11) Pandey, M. P.; Kim, C. S. Lignin Depolymerization and Conversion: A Review of Thermochemical Methods. *Chem. Eng. Technol.* **2011**, *34*, 29−41.
(12) Anderson, E. M.; Stone, M. L.; Katahira, R.; Reed, M.; Beckham, G. T.; Román-Leshkov, Y. Flowthrough Reductive Catalytic Fractionation of Biomass. *Joule* **2017**, *1*, 613−622.
(13) Anderson, E. M.; Stone, M. L.; Hülsey, M. J.; Beckham, G. T.; Román-Leshkov, Y. Kinetic Studies of Lignin Solvolysis and Reduction by Reductive Catalytic Fractionation Decoupled in Flow-through Reactors. *ACS Sustainable Chem. Eng.* **2018**, *6*, 7951−7959.
(14) Zakzeski, J.; Bruijnincx, P. C.; Jongerius, A. L.; Weckhuysen, B. M. The Catalytic Valorization of Lignin for the Production of Renewable Chemicals. *Chem. Rev.* **2010**, *110*, 3552−3599.
(15) Galkin, M. V.; Samec, J. S. Lignin Valorization through Catalytic Lignocellulose Fractionation: A Fundamental Platform for the Future Biorefinery. *ChemSusChem* **2016**, *9*, 1544−1558.
(16) Phongpreecha, T.; Hool, N. C.; Stoklosa, R. J.; Klett, A. S.; Foster, C. E.; Bhalla, A.; Holmes, D.; Thies, M. C.; Hodge, D. B. Predicting Lignin Depolymerization Yields from Quantifiable Properties Using Fractionated Biorefinery Lignins. *Green Chem.* **2017**, *19*, 5131−5143.

(17) Anderson, E. M.; Stone, M. L.; Katahira, R.; Reed, M.; Muchero, W.; Ramirez, K. J.; Beckham, G. T.; Román-Leshkov, Y. Differences in S/G Ratio in Natural Poplar Variants Do Not Predict Catalytic Depolymerization Monomer Yields. *Nat. Commun.* **2019**, *10* (2033), 09986.
(18) Das, A.; Rahimi, A.; Ulbrich, A.; Alherech, M.; Motagamwala, A. H.; Bhalla, A.; da Costa Sousa, L.; Balan, V.; Dumesic, J. A.; Hegg, E. L. Lignin Conversion to Low-Molecular-Weight Aromatics Via an Aerobic Oxidation-Hydrolysis Sequence: Comparison of Different Lignin Sources. *ACS Sustainable Chem. Eng.* **2018**, *6*, 3367−3374.
(19) Liu, C.-J. Deciphering the Enigma of Lignification: Precursor Transport, Oxidation, and the Topochemistry of Lignin Assembly. *Mol. Plant* **2012**, *5*, 304−317.
(20) Ralph, J.; Peng, J.; Lu, F.; Hatfield, R. D.; Helm, R. F. Are Lignins Optically Active? *J. Agric. Food Chem.* **1999**, *47*, 2991−2996.
(21) Mottiar, Y.; Vanholme, R.; Boerjan, W.; Ralph, J.; Mansfield, S. D. Designer Lignins: Harnessing the Plasticity of Lignification. *Curr. Opin. Biotechnol.* **2016**, *37*, 190−200.
(22) Adler, E. Structural Elements of Lignin. *Ind. Eng. Chem.* **1957**, *49*, 1377−1383.
(23) Freudenberg, K. Lignin: Its Constitution and Formation from *p*-Hydroxycinnamyl Alcohols. *Science* **1965**, *148*, 595−600.
(24) Sakakibara, A. A Structural Model of Softwood Lignin. *Wood Sci. Technol.* **1980**, *14*, 89−100.
(25) Glasser, W. G.; Glasser, H. R.; Morohoshi, N. Simulation of Reactions with Lignin by Computer (SIMREL). 6. Interpretation of Primary Experimental Analysis Data ("Analysis Program"). *Macromolecules* **1981**, *14*, 253−262.
(26) Yanez, A. J.; Li, W.; Mabon, R.; Broadbelt, L. J. A Stochastic Method to Generate Libraries of Structural Representations of Lignin. *Energy Fuels* **2016**, *30*, 5835−5845.
(27) Dellon, L. D.; Yanez, A. J.; Li, W.; Mabon, R.; Broadbelt, L. J. Computational Generation of Lignin Libraries from Diverse Biomass Sources. *Energy Fuels* **2017**, *31*, 8263−8274.
(28) Yanez, A. J.; Natarajan, P.; Li, W.; Mabon, R.; Broadbelt, L. J. Coupled Structural and Kinetic Model of Lignin Fast Pyrolysis. *Energy Fuels* **2018**, *32*, 1822−1830.
(29) van Parijs, F. R.; Morreel, K.; Ralph, J.; Boerjan, W.; Merks, R. M. Modeling Lignin Polymerization. Part 1: Simulation Model of Dehydrogenation Polymers. *Plant Physiol.* **2010**, *153*, 1332−1344.
(30) Tobimatsu, Y.; Schuetz, M. Lignin Polymerization: How Do Plants Manage the Chemistry So Well? *Curr. Opin. Biotechnol.* **2019**, *56*, 75−81.
(31) Tanahashi, M.; Takeuchi, H.; Higuchi, T. Dehydrogenative Polymerization of 3, 5-Disubstituted *p*-Coumaryl Alcohols. *Wood Res. (Kyoto, Jpn.)* **1976**, *61*, 44−53.
(32) Katayama, Y.; Fukuzumi, T. Enzymatic Synthesis of Three Lignin-Related Dimers by an Improved Peroxidase-Hydrogen Peroxide System. *Mokuzai Gakkaishi* **1978**, *24*, 664−667.
(33) Tanahashi, M.; Higuchi, T. Dehydrogenative Polymerization of Monolignols by Peroxidase and H2O2 in a Dialysis Tube. I.: Preparation of Highly Polymerized DHPs. *Wood Res. (Kyoto, Jpn.)* **1981**, *67*, 29−42.
(34) Saake, B.; Argyropoulos, D. S.; Beinhoff, O.; Faix, O. A Comparison of Lignin Polymer Models (DHPs) and Lignins by 31P NMR Spectroscopy. *Phytochemistry* **1996**, *43*, 499−507.
(35) Syrjänen, K.; Brunow, G. Oxidative Cross Coupling of *p*-Hydroxycinnamic Alcohols with Dimeric Arylglycerol *β*-Aryl Ether Lignin Model Compounds. The Effect of Oxidation Potentials. *J. Chem. Soc., Perkin Trans. 1* **1998**, *1*, 3425−3430.
(36) Syrjänen, K.; Brunow, G. Regioselectivity in Lignin Biosynthesis. The Influence of Dimerization and Cross-Coupling. *J. Chem. Soc., Perkin Trans.* **2000**, *1*, 183−187.
(37) Tobimatsu, Y.; Takano, T.; Kamitakahara, H.; Nakatsubo, F. Studies on the Dehydrogenative Polymerizations of Monolignol *β*-Glycosides. Part 2: Horseradish Peroxidase-Catalyzed Dehydrogenative Polymerization of Isoconiferin. *Holzforschung* **2006**, *60*, 513−518.
(38) Beste, A.; Buchanan, A., III Computational Study of Bond Dissociation Enthalpies for Lignin Model Compounds. Substituent Effects in Phenethyl Phenyl Ethers. *J. Org. Chem.* **2009**, *74*, 2837−2841.
(39) Younker, J. M.; Beste, A.; Buchanan, A., III Computational Study of Bond Dissociation Enthalpies for Substituted *β*-O-4 Lignin Model Compounds. *ChemPhysChem* **2011**, *12*, 3556−3565.
(40) Kim, S.; Chmely, S. C.; Nimlos, M. R.; Bomble, Y. J.; Foust, T. D.; Paton, R. S.; Beckham, G. T. Computational Study of Bond Dissociation Enthalpies for a Large Range of Native and Modified Lignins. *J. Phys. Chem. Lett.* **2011**, *2*, 2846−2852.
(41) Parthasarathi, R.; Romero, R. A.; Redondo, A.; Gnanakaran, S. Theoretical Study of the Remarkably Diverse Linkages in Lignin. *J. Phys. Chem. Lett.* **2011**, *2*, 2660−2666.
(42) Younker, J. M.; Beste, A.; Buchanan, A., III Computational Study of Bond Dissociation Enthalpies for Lignin Model Compounds: *β*-5 Arylcoumaran. *Chem. Phys. Lett.* **2012**, *545*, 100−106.
(43) Elder, T. Bond Dissociation Enthalpies of a Dibenzodioxocin Lignin Model Compound. *Energy Fuels* **2013**, *27*, 4785−4790.
(44) Elder, T. Bond Dissociation Enthalpies of a Pinoresinol Lignin Model Compound. *Energy Fuels* **2014**, *28*, 1175−1182.
(45) Elder, T.; Berstis, L.; Beckham, G. T.; Crowley, M. F. Coupling and Reactions of 5-Hydroxyconiferyl Alcohol in Lignin Formation. *J. Agric. Food Chem.* **2016**, *64*, 4742−4750.
(46) Elder, T.; Berstis, L.; Beckham, G. T.; Crowley, M. F. Density Functional Theory Study of Spirodienone Stereoisomers in Lignin. *ACS Sustainable Chem. Eng.* **2017**, *5*, 7188−7194.
(47) Gierer, J.; Norén, I. Oxidative Pretreatment of Pine Wood to Facilitate Delignification During Kraft Pulping. *Holzforschung* **1982**, *36*, 123−130.
(48) Sangha, A. K.; Davison, B. H.; Standaert, R. F.; Davis, M. F.; Smith, J. C.; Parks, J. M. Chemical Factors That Control Lignin Polymerization. *J. Phys. Chem. B* **2014**, *118*, 164−170.
(49) Watts, H. D.; Mohamed, M. N. A.; Kubicki, J. D. Evaluation of Potential Reaction Mechanisms Leading to the Formation of Coniferyl Alcohol *α*-Linkages in Lignin: A Density Functional Theory Study. *Phys. Chem. Chem. Phys.* **2011**, *13*, 20974−20985.
(50) Sangha, A. K.; Parks, J. M.; Standaert, R. F.; Ziebell, A.; Davis, M.; Smith, J. C. Radical Coupling Reactions in Lignin Synthesis: A Density Functional Theory Study. *J. Phys. Chem. B* **2012**, *116*, 4760−4768.
(51) Durbeej, B.; Eriksson, L. A. Formation of *β*-O-4 Lignin Models-a Theoretical Study. *Holzforschung* **2003**, *57*, 466−478.
(52) Shigematsu, M.; Kobayashi, T.; Taguchi, H.; Tanahashi, M. Transition State Leading to *β*-O' Quinonemethide Intermediate of *p*-Coumaryl Alcohol Analyzed by Semi-Empirical Molecular Orbital Calculation. *J. Wood Sci.* **2006**, *52*, 128−133.
(53) Neese, F. The ORCA Program System. *Wiley Interdiscip. Rev.: Comput. Mol. Sci.* **2012**, *2*, 73−78.
(54) Becke, A. D. Density-Functional Exchange-Energy Approximation with Correct Asymptotic Behavior. *Phys. Rev. A: At., Mol., Opt. Phys.* **1988**, *38*, 3098−3100.
(55) Becke, A. D. Density-Functional Thermochemistry. III. The Role of Exact Exchange. *J. Chem. Phys.* **1993**, *98*, 5648−5652.
(56) Stephens, P. J.; Devlin, F. J.; Chabalowski, C. F.; Frisch, M. J. Ab Initio Calculation of Vibrational Absorption and Circular Dichroism Spectra Using Density Functional Force Fields. *J. Phys. Chem.* **1994**, *98*, 11623−11627.
(57) Grimme, S.; Antony, J.; Ehrlich, S.; Krieg, H. A Consistent and Accurate Ab Initio Parametrization of Density Functional Dispersion Correction (DFT-D) for the 94 Elements H-Pu. *J. Chem. Phys.* **2010**, *132*, 154104.
(58) Weigend, F.; Ahlrichs, R. Balanced Basis Sets of Split Valence, Triple Zeta Valence and Quadruple Zeta Valence Quality for H to Rn: Design and Assessment of Accuracy. *Phys. Chem. Chem. Phys.* **2005**, *7*, 3297−3305.
(59) Zhao, Y.; Truhlar, D. G. The M06 Suite of Density Functionals for Main Group Thermochemistry, Thermochemical Kinetics, Noncovalent Interactions, Excited States, and Transition Elements:

DOI: 10.1021/acssuschemeng.9b02506
ACS Sustainable Chem. Eng. XXXX, XXX, XXX−XXX

Two New Functionals and Systematic Testing of Four M06-Class Functionals and 12 Other Functionals. *Theor. Chem. Acc.* **2008**, *120*, 215−241.
(60) Cossi, M.; Rega, N.; Scalmani, G.; Barone, V. Energies, Structures, and Electronic Properties of Molecules in Solution with the C-PCM Solvation Model. *J. Comput. Chem.* **2003**, *24*, 669−681.
(61) Husch, T.; Seebach, D.; Beck, A. K.; Reiher, M. Rigorous Conformational Analysis of Pyrrolidine Enamines with Relevance to Organocatalysis. *Helv. Chim. Acta* **2017**, *100*, No. e1700182.
(62) Yu, Y. B.; Privalov, P. L.; Hodges, R. S. Contribution of Translational and Rotational Motions to Molecular Association in Aqueous Solution. *Biophys. J.* **2001**, *81*, 1632−1642.
(63) Bell, R. P. The Theory of Reactions Involving Proton Transfers. *Proc. R. Soc. London A* **1936**, *154*, 414−429.
(64) Evans, M.; Polanyi, M. Further Considerations on the Thermodynamics of Chemical Equilibria and Reaction Rates. *Trans. Faraday Soc.* **1936**, *32*, 1333−1360.
(65) Fan, T.; Zhan, S.; Ahlquist, M. S. Why Is There a Barrier in the Coupling of Two Radicals in the Water Oxidation Reaction? *ACS Catal.* **2016**, *6*, 8308−8312.
(66) Bickelhaupt, F. M.; Houk, K. N. Analyzing Reaction Rates with the Distortion/Interaction-Activation Strain Model. *Angew. Chem., Int. Ed.* **2017**, *56*, 10070−10086.
(67) Cheong, P. H.-Y.; Paton, R. S.; Bronner, S. M.; Im, G.-Y. J.; Garg, N. K.; Houk, K. Indolyne and Aryne Distortions and Nucleophilic Regioselectivites. *J. Am. Chem. Soc.* **2010**, *132*, 1267−1269.
(68) Ralph, J.; Brunow, G.; Harris, P. J.; Dixon, R. A.; Schatz, P. F.; Boerjan, W., Lignification: Are Lignins Biosynthesized Via Simple Combinatorial Chemistry or Via Proteinaceous Control and Template Replication. In *Recent Advances in Polyphenol Research*, Daayf, F., El Hadrami, A., Adam, L., Ballance, G. M., Eds.; Wiley-Blackwell Publishing: Oxford, UK, 2008; Vol. *1*, pp 36−66.
(69) Erickson, M.; Miksche, G. E.; Mukherjee, A. D.; Nicholson, D. G.; Southern, J. T. Modellversuche Zur Bildung Des Lignins. I. Enzymatische Dehydrierung Von Zimtalkoholen in Gegenwart Von 4-Alkylphenolen. *Acta Chem. Scand.* **1972**, *26*, 3085−3096.
(70) Warinowski, T.; Koutaniemi, S.; Kärkönen, A.; Sundberg, I.; Toikka, M.; Simola, L. K.; Kilpeläinen, I.; Teeri, T. H. Peroxidases Bound to the Growing Lignin Polymer Produce Natural Like Extracellular Lignin in a Cell Culture of Norway Spruce. *Front. Plant Sci.* **2016**, *7*, 01523.
(71) Méchin, V.; Baumberger, S.; Pollet, B.; Lapierre, C. Peroxidase Activity Can Dictate the *in vitro* Lignin Dehydrogenative Polymer Structure. *Phytochemistry* **2007**, *68*, 571−579.
(72) Sasaki, S.; Nishida, T.; Tsutsumi, Y.; Kondo, R. Lignin Dehydrogenative Polymerization Mechanism: A Poplar Cell Wall Peroxidase Directly Oxidizes Polymer Lignin and Produces in vitro Dehydrogenative Polymer Rich in β-O-4 Linkage. *FEBS Lett.* **2004**, *562*, 197−201.
(73) Hatfield, R.; Ralph, J.; Grabber, J. H. A Potential Role for Sinapyl *p*-Coumarate as a Radical Transfer Mechanism in Grass Lignin Formation. *Planta* **2008**, *228*, 919−928.
(74) Mayer, J. M.; Hrovat, D. A.; Thomas, J. L.; Borden, W. T. Proton-Coupled Electron Transfer Versus Hydrogen Atom Transfer in Benzyl/Toluene, Methoxyl/Methanol, and Phenoxyl/Phenol Self-Exchange Reactions. *J. Am. Chem. Soc.* **2002**, *124*, 11142−11147.
(75) Ralph, J.; Bunzel, M.; Marita, J. M.; Hatfield, R. D.; Lu, F.; Kim, H.; Schatz, P. F.; Grabber, J. H.; Steinhart, H. Peroxidase-Dependent Cross-Linking Reactions of *p*-Hydroxycinnamates in Plant Cell Walls. *Phytochem. Rev.* **2004**, *3*, 79−96.
(76) Yue, F.; Lu, F.; Ralph, S.; Ralph, J. Identification of 4-O-5-Units in Softwood Lignins Via Definitive Lignin Models and NMR. *Biomacromolecules* **2016**, *17*, 1909−1920.
(77) Tohmura, S.-I.; Argyropoulos, D. S. Determination of Arylglycerol-β-aryl Ethers and Other Linkages in Lignins Using DFRC/31P NMR. *J. Agric. Food Chem.* **2001**, *49*, 536−542.
(78) Wagner, A.; Donaldson, L.; Kim, H.; Phillips, L.; Flint, H.; Steward, D.; Torr, K.; Koch, G.; Schmitt, U.; Ralph, J. Suppression of 4-Coumarate-CoA Ligase in the Coniferous Gymnosperm *Pinus radiata*. *Plant Physiol.* **2009**, *149*, 370−383.
(79) Orella, M.; Gani, T.; Vermaas, J. V.; Stone, M.; Anderson, E.; Beckham, G.; Brushett, F.; Román-Leshkov, Y. LIGNIN-KMC: A Toolkit for Simulating Lignin Biosynthesis. *ChemRxiv* **2019**, 8178722.

DOI: 10.1021/acssuschemeng.9b02506
ACS Sustainable Chem. Eng. XXXX, XXX, XXX−XXX